Efficient Path Planning Algorithm for Additive Manufacturing Systems

Bradley Thompson and Hwan-Sik Yoon

***Abstract*— Recent additive manufacturing technologies, such as 3-D printing and printed electronics, require constant speed motion for consistent material deposition. In this paper, a new path planning algorithm is developed for an XY-motion stage with an emphasis on aerosol printing. The continuous aerosol stream provided by the printing nozzle requires constant velocity in relative motion of a substrate to evenly deposit inks. During transitioning between print segments, a shutter prevents the aerosol from reaching the substrate, therefore wasting material. The proposed path planning algorithm can control motion of an XY stage for an arbitrary printing path and desired velocity while minimizing material waste. Linear segments with parabolic blends (LSPBs) trajectory planning is used during printing, and minimum time trajectory (MTT) planning is used during printer transition. Simulation results show that combining LSPB with MTT can minimize the printing time while following the desired path.**

***Index Terms*— Additive manufacturing, aerosol printing, linear segments with parabolic blends (LSPBs), minimum time trajectory (MTT).**

I. Introduction

ADDITIVE manufacturing of 3-D parts and electronic devices is gaining increasing attention. Instead of relying on removal of materials to form 3-D solid objects or multilayered electronic devices, 3-D printing and printed electronic technologies utilize additive processes where successive layers of materials are deposited in a desired pattern [1], [2]. The 3-D printing technology can be applied to build numerous items that range from household goods to industrial or defense system components [3]. In much the same way that the 3-D printing can produce solid objects, printed electronics technology can be used to fabricate various electronic components, such as resistors, conductors, transistors, and sensors [4]–[10]. For example, researchers have demonstrated that mechanical strain sensors can be fabricated using printed electronics technology [11]–[15].

For most of the 3-D printing techniques, it is desirable that the extrusion deposition head or workpiece maintain constant-speed motion to evenly deposit materials [1]. This is because printer heads usually dispense materials at a constant feed rate, and thus, variation in printer head speed could result in change in deposition thickness. In the field of printed electronics, aerosol printing has been proven to be an effective method for fabricating numerous macroelectronic devices. In aerosol printing, a gas transports ink droplets to a substrate through a nozzle. Since the flow of the aerosol stream is continuous, the XY-motion stage must maintain a near constant speed to evenly deposit materials on a substrate. A mechanical shutter is typically utilized to block aerosol stream during transition of the printer head because the produced aerosol cannot be started or stopped abruptly. To minimize the volume of captured and wasted ink, the transition time must be minimized.

In this paper, a new path planning algorithm is developed for an XY-motion stage based on two motion control methods: linear segments with parabolic blends (LSPBs) and minimum time trajectory (MTT). LSPB trajectory planning maps the motion of an actuator using a trapezoidal velocity profile consisting of two acceleration or deceleration regions and a constant velocity section. Therefore, position, when plotted as a function of time, becomes a set of LSPBs [16]. An MTT method minimizes transition time with a triangular velocity profile or a LSPB trajectory limited by an actuator's maximum velocity [16].

Although the fundamental theory is available regarding control of robotic manipulators, no work has been published on the constant-speed control of a printer head or a motion stage in additive manufacturing systems. Thus, the purpose of this paper is to develop an effective path planning algorithm for additive manufacturing systems with a special emphasis on an aerosol printing system.

To control the motion stage, an algorithm plans the trajectory before printing, and when executed, the printing procedure progresses autonomously. Although the path planning algorithm presented in this paper is designed for an aerosol printer, it is equally well suited in other types of additive manufacturing systems. The developed path planning algorithm is applied to arbitrary printing layouts, and the results are presented and discussed. The results show that the algorithm can be used to schedule the velocity and position of an XY-motion stage such that the system can accomplish an assigned printing task in a time-efficient manner.

II. XY-Motion Stage

A. System Description

The additive manufacturing system considered in this paper is an aerosol printer. Although inkjet was first used in printed

Manuscript received August 21, 2013; revised May 13, 2014; accepted July 8, 2014. Date of publication July 29, 2014; date of current version September 4, 2014. Recommended for publication by Associate Editor S. J. Mason upon evaluation of reviewers' comments.

The authors are with the Department of Mechanical Engineering, University of Alabama, Tuscaloosa, AL 35487-0276 USA (e-mail: bathompson21@gmail.com; hyoon@eng.ua.edu).

Color versions of one or more of the figures in this paper are available online at http://ieeexplore.ieee.org.

Digital Object Identifier 10.1109/TCPMT.2014.2338791

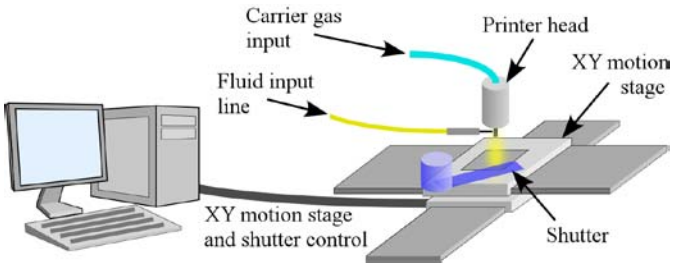

Fig. 1. Ultrasonic atomizer nozzle printer configuration.

electronics, aerosol printing has become widely accepted due to numerous advantages over inkjet printing. Aerosol printing drastically reduces clogging issues, is less dependent on the substrate surface condition, and deposits inks more evenly due to fine aerosol particles.

Whereas an inkjet or drop-on-demand printer deposits materials by precisely controlling drop expulsion time, an aerosol stream in an aerosol printer cannot be controlled by abrupt actuations. To accurately control duration of aerosol deposition, a mechanical shutter must be used. The shutter blocks the aerosol stream during transitions and allows flow when following a desired print path. Unlike an inkjet printer, the closed shutter results in a portion of the deposition material being wasted during the printing process. The volume of fluid captured by the shutter can be minimized with careful planning and minimization of transition time.

An example of an aerosol printing system is shown in Fig. 1. The system consists of an XY-motion stage, a printer head, and a mechanical shutter. Once the user inputs a desired printing pattern, control software automates the printing process by controlling XY motion, atomization, and shutter actuations. Path planning provides the XY stage with position and velocities that minimize print time, and then, the XY stage executes the required motion for printing.

B. Motion Stage Control

Since acceleration and deceleration of the aerosol printer head will disrupt the aerosol stream, and therefore deposit materials inconsistently, the substrate is moved by the XY-motion stage while the printer head remains fixed. Therefore, precise control of the position and velocity of the XY-motion stage is important to deposit materials at desired locations on the substrate. Printing speed determined by the user dictates the volume of liquid deposited per unit area. By translating the substrate at a specified speed, the thickness of the deposited ink can be determined, assuming the volumetric flow rate of the fluid contained in the aerosol to be steady.

III. Motion Control Method I: LSPBs

In this paper, it is assumed that two motor controllers utilize a trapezoidal velocity profile to control the motion of the XY stage. Such controllers are commercially available from manufacturers of motion stages. A trapezoidal velocity profile consists of an initial linear increase in velocity, then a constant velocity section, and a final linear decrease in velocity. By integrating the velocity profile, position $q(t)$, naturally becomes a set of quadratic and linear functions of time, giving the name LSPBs. Acceleration, velocity, and position profiles for an example LSPB trajectory are shown in Fig. 2. In the figure, the trajectory planned between two waypoints, q_0 and q_1, begins at an initial velocity v_0, accelerates to v_c, remains at a constant velocity, and finally decelerates to the final velocity v_1. The first acceleration region occurs between the initial time t_0 and the first blend time t_{b0}. Velocity then remains constant until the second blend time t_{b1}. Between t_{b1} and the end time t_1 acceleration or deceleration takes place to reach the final velocity v_1.

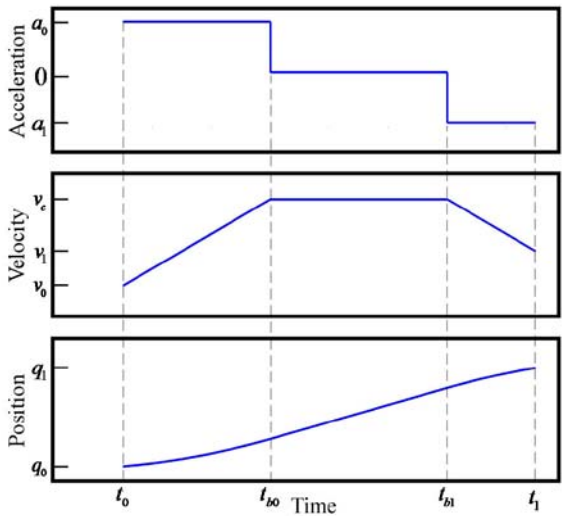

Fig. 2. Acceleration, velocity, and position profiles for an example LSPB trajectory between two points.

A. Mathematical Description

To plan a trajectory $q(t)$ between two points using the LSPB method, the following boundary conditions are specified:

$$q(t_0) = q_0 \tag{1}$$

$$q(t_1) = q_1 \tag{2}$$

$$\dot{q}(t_0) = v(t_0) = v_0 \tag{3}$$

and

$$\dot{q}(t_1) = v(t_1) = v_1 \tag{4}$$

where the start time t_0 and end time t_1 are known. Assuming the acceleration values a_0 and a_1 are known, the three remaining variables, t_{b0}, t_{b1}, and v_c must be derived according to the trajectory's boundary conditions. By integrating the acceleration profile, the following relationships for the blend times can be determined:

$$t_{b0} = \frac{v_c - v_0}{a_0} + t_0 \tag{5}$$

$$t_{b1} = \frac{v_c - v_1}{a_1} + t_1. \tag{6}$$

By integrating the trapezoidal velocity profile, the final position q_1 can be related to other variables as follows:

$$q_1 = q_0 + \frac{v_c + v_0}{2}(t_{b0} - t_0) + v_c(t_{b1} - t_{b0}) + \frac{v_c + v_1}{2}(t_1 - t_{b1}). \tag{7}$$

After substituting (5) and (6) into (7), v_c can be obtained by solving the resulting quadratic equation assuming a_0 does not equal a_1. The peak constant velocity v_c is given by

$$v_c = \frac{a_0 a_1}{a_1 - a_0}\left(\frac{v_0}{a_0} - \frac{v_1}{a_1} + t_1 - t_0\right) \pm \frac{a_0 a_1}{a_1 - a_0} \cdot \sqrt{\left(\frac{v_0}{a_0} - \frac{v_1}{a_1} + t_1 - t_0\right)^2 - \left(\frac{1}{a_1} - \frac{1}{a_0}\right)\left(\frac{v_1^2}{a_1} - \frac{v_0^2}{a_0} + 2q_0 - 2q_1\right)}. \tag{8}$$

When a_0 and a_1 are equal, the expression for v_c becomes

$$v_c = \frac{a_1(q_1 - q_0) + \frac{1}{2}(v_0^2 - v_1^2)}{v_0 - v_1 + a_1(t_1 + t_0)}. \tag{9}$$

The obtained constant velocity v_c can now be used to calculate the unknown blend times with (5) and (6).

Although the above equation derivation assumes known a_0 and a_1, the directions of the accelerations depend on each individual printing pattern and are generally unknown. Therefore, different combinations of a_0 and a_1 must be considered to find a real and suitable solution. For simplicity, a_0 and a_1 are restricted to

$$|a_0| = |a_1| = \alpha \quad \text{where} \quad \alpha > 0. \tag{10}$$

The imposed constraint decreases an infinite number of possible solutions to four cases. Using (8) and (9), v_c can be determined for four different cases.

Case I: $a_0 = \alpha$ and $a_1 = -\alpha$

$$v_{c1}, v_{c2} = \frac{1}{2}\alpha\left[\left(\frac{v_0 + v_1}{\alpha} + t_1 - t_0\right) \pm \sqrt{\gamma_1}\right] \tag{11}$$

where

$$\gamma_1 = \left(\frac{v_0 + v_1}{\alpha} + t_1 - t_0\right)^2 + \frac{2}{\alpha}\left(-\frac{v_0^2 + v_1^2}{\alpha} + 2q_0 - 2q_1\right). \tag{12}$$

Case II: $a_0 = -\alpha$ and $a_1 = \alpha$

$$v_{c3}, v_{c4} = -\frac{1}{2}\alpha\left[\left(-\frac{v_0 + v_1}{\alpha} + t_1 - t_0\right) \pm \sqrt{\gamma_2}\right] \tag{13}$$

where

$$\gamma_2 = \left(-\frac{v_0 + v_1}{\alpha} + t_1 - t_0\right)^2 - \frac{2}{\alpha}\left(\frac{v_0^2 + v_1^2}{\alpha} + 2q_0 - 2q_1\right). \tag{14}$$

Case III: $a_0 = \alpha$ and $a_1 = \alpha$

$$v_{c5} = \frac{\alpha(q_1 - q_0) + \frac{1}{2}(v_0^2 - v_1^2)}{v_0 - v_1 + \alpha(t_1 + t_0)}. \tag{15}$$

Case IV: $a_0 = -\alpha$ and $a_1 = -\alpha$

$$v_{c6} = \frac{-\alpha(q_1 - q_0) + \frac{1}{2}(v_0^2 - v_1^2)}{v_0 - v_1 - \alpha(t_1 + t_0)}. \tag{16}$$

Because cases I and II have two possible solutions each, the four cases produce six total possible solutions: v_{c1}, v_{c2}, v_{c3}, v_{c4}, v_{c5}, and v_{c6}. The appropriate solution or solutions are determined by checking the validity of the corresponding blend times, t_{b0} and t_{b1}, and omitting imaginary solutions. The solutions for t_{b0}, t_{b1}, and v_c are valid if and only if they satisfy the following constraints:

$$\text{imag}(v_c) = 0 \tag{17}$$

and

$$t_0 \le t_{b0} \le t_{b1} \le t_1. \tag{18}$$

If none of the six possible solutions satisfy both constraints, no solution exists for the given set of constraints. If this is the case, a plausible solution can only be reached by changing one or more of the trajectory boundary conditions or increasing the time allotted to complete the trajectory.

B. LSPB Algorithm

For the purpose of tracking a desired print path, the LSPB trajectory described in the previous section is implemented. Each print segment, which will be discussed later, is defined by two points and a desired average velocity. From the given information, the initial position, initial velocity, final position, final velocity, and elapsed time can be derived for the x- and y-directions. Therefore, each degree of freedom operates independently. Due to independence, an LSPB trajectory planning algorithm for a single degree of freedom can be developed and employed for both motion stages.

As shown in the flowchart in Fig. 3, the algorithm calculates blend times and constant velocity (t_{b0}, t_{b1}, and v_c) based on given trajectory boundary conditions (q_0, q_1, v_0, v_1, t_0, and t_1) for a single degree of freedom. Since one solution that satisfies the constraints in (17) and (18) can be returned out of six possible solutions, computation time can be reduced by checking the validity of each obtained solution before continuing. To avoid an imaginary number in the solution, γ_1 is calculated first. If $\gamma_1 \ge 0$, the solutions, v_{c1} and v_{c2}, are real, but if $\gamma_1 < 0$, the first two solutions are discarded. If the constraint given by (17) is satisfied, v_{c1} and the corresponding blend times are calculated and verified. If the first solution meets both constraints, the results are returned. Otherwise, v_{c2} is considered. The next two solutions, v_{c3} and v_{c4}, are calculated and checked in a similar manner. For the final two solutions, v_{c5} and v_{c6}, (17) does not apply but must satisfy the constraint in (18). If (18) cannot be satisfied, no solution will be returned. If this situation occurs, one or more of the trajectory boundary conditions need to be changed to obtain a valid solution.

IV. Motion Control Method II: MTT

Translating from one point to another as quickly as possible can be beneficial in many applications. In the case of an aerosol printer, decreasing the time required to travel between printing sections reduces the amount of wasted ink, time required to print, and corresponding cost. Therefore, an MTT planning method is derived in this section. The MTT is a special case of LSPB path planning where $t_{b0} = t_{b1}$ and the end time t_1 must be determined. By equating t_{b0} to t_{b1}, a peak velocity v_p is reached at a single blend time t_b, and the resulting triangular velocity profile shown in Fig. 4 minimizes transition time.

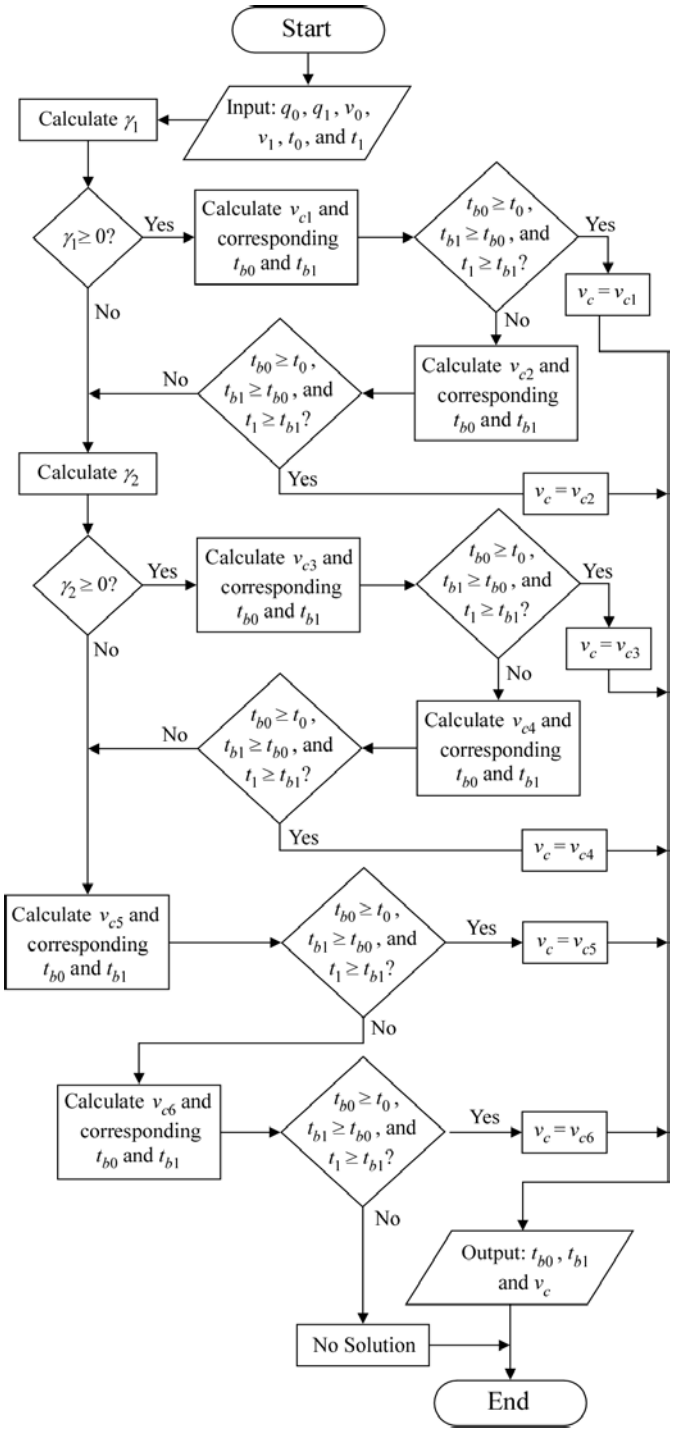

Fig. 3. Flowchart for LSPB trajectory planning for single degree of freedom motion control.

A. MTT Algorithm for Single Degree of Freedom Motion

A minimal time trajectory must satisfy the boundary conditions given in (1) to (4) within a minimal time. Therefore, the end time t_1 and the blend time t_b must be determined. Equations for the unknown time values

$$t_b = \frac{v_p - v_0}{a_0} + t_0 \tag{19}$$

and

$$t_1 = \frac{v_1 - v_p}{a_1} + t_b \tag{20}$$

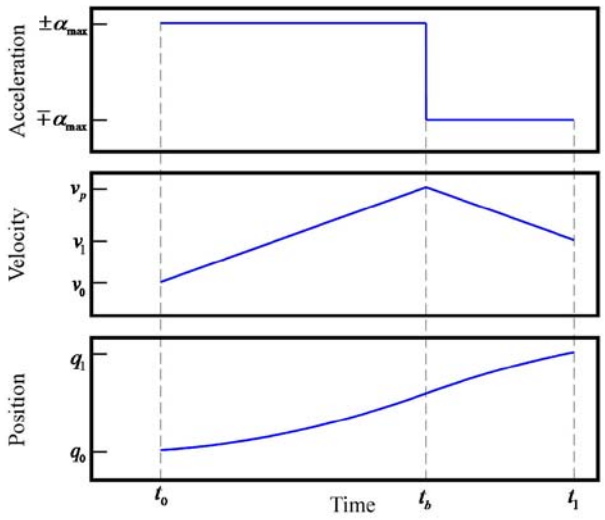

Fig. 4. Acceleration, velocity, and position profiles for an example MTT between two points.

can be established by integrating the trajectory accelerations.

By integrating the velocity profiles, the relationship

$$q_1 = q_0 + \frac{v_p + v_0}{2}(t_b - t_0) + \frac{v_p + v_1}{2}(t_1 - t_b) \tag{21}$$

completes the set of equations. For the typical case when $a_0 \neq a_1$, the peak velocity v_p can be obtained by substituting (19) and (20) into (21) and solving for v_p, which results in

$$v_p = \pm\sqrt{\frac{2a_0a_1(q_1 - q_0) + a_1v_0^2 + a_0v_1^2}{a_1 - a_0}}. \tag{22}$$

To maximize v_p and thus minimize the transition time, the magnitudes of the accelerations a_0 and a_1 are substituted by the absolute maximum acceleration $\alpha_{\max}$, which is specified before the path scheduling. Then, the following two cases can be considered for calculating the peak velocity.

Case I: $a_0 = \alpha_{\max}$ and $a_1 = -\alpha_{\max}$

$$v_{p1}, v_{p2} = \pm\sqrt{\lambda_1} \tag{23}$$

where

$$\lambda_1 = \alpha_{\max}(q_1 - q_0) + \frac{1}{2}(v_1^2 - v_0^2). \tag{24}$$

Case II: $a_0 = -\alpha_{\max}$ and $a_1 = \alpha_{\max}$

$$v_{p3}, v_{p4} = \pm\sqrt{\lambda_2} \tag{25}$$

where

$$\lambda_2 = \alpha_{\max}(q_0 - q_1) + \frac{1}{2}(v_0^2 - v_1^2). \tag{26}$$

The two cases produce four possible solutions for v_p, t_b, and t_1. To determine a suitable solution or solutions, the constraints

$$\text{imag}(v_p) = 0 \tag{27}$$

and

$$t_0 \leq t_b \leq t_1 \tag{28}$$

must be satisfied. Because elapsed time is not specified, at least one solution for all boundary conditions will exist.

A situation may arise when the calculated peak velocity exceeds an actuator's maximum velocity. If

$$|v_p| > |v_{\max}| \tag{29}$$

where $|v_{\max}|$ is the maximum possible speed of a motion stage, then the LSPB method described earlier must be utilized. In this case, t_{b0}, t_{b1}, and t_1 must be determined, and v_c is set to $v_{\max}$. Substituting (5) and (6) into (7), the end time can be determined by

$$t_1 = \frac{q_1 - q_0}{v_{\max}} + v_{\max}\left(\frac{1}{2a_0} - \frac{1}{2a_1}\right) + \frac{v_1}{a_1} - \frac{v_0}{a_0} + \frac{v_0^2}{2a_0 v_{\max}} - \frac{v_1^2}{2a_1 v_{\max}} + t_0. \tag{30}$$

Because the maximum possible speed can never be exceeded, the boundary velocities must be constrained, such that

$$|v_0| \le |v_{\max}| \tag{31}$$

and

$$|v_1| \le |v_{\max}|. \tag{32}$$

Therefore, it can be concluded that

$$v_{\max} = \operatorname{sgn}(q_1 - q_0)\,|v_{\max}| \tag{33}$$

$$a_0 = \operatorname{sgn}(q_1 - q_0)\;\alpha_{\max} \tag{34}$$

and

$$a_1 = -\operatorname{sgn}(q_1 - q_0)\;\alpha_{\max}. \tag{35}$$

With the given constraints, t_{b0}, t_1, and t_{b1} can now be determined for every situation by the following set of equations:

$$t_{b0} = \frac{|v_{\max}| - \operatorname{sgn}(q_1 - q_0)\,v_0}{\alpha_{\max}} + t_0, \tag{36}$$

$$t_1 = \operatorname{sgn}(q_1 - q_0)\cdot\left[\frac{q_1 - q_0}{|v_{\max}|} + |v_{\max}|\left(\frac{1}{2\alpha_{\max}} + \frac{1}{2\alpha_{\max}}\right) - \frac{v_1}{\alpha_{\max}} - \frac{v_0}{\alpha_{\max}}\right] + \frac{v_1^2 + v_0^2}{2\alpha_{\max}\,|v_{\max}|} + t_0 \tag{37}$$

and

$$t_{b1} = \frac{\operatorname{sgn}(q_1 - q_0)\,v_1 - |v_{\max}|}{\alpha_{\max}} + t_1. \tag{38}$$

To automate the planning process for a MTT, an algorithm is developed for single degree of freedom motion. Referring to the flowchart in Fig. 5, the boundary conditions (q_0, q_1, v_0, and v_1) and start time t_0 enter the function, and the algorithm produces the corresponding end time, blend times, and constant velocity (t_1, t_{b0}, t_{b1}, and v_c). The algorithm first assumes a triangular velocity profile where a single blend time t_b is determined. To avoid obtaining an imaginary solution, λ_1 should be calculated and examined. If $\lambda_1 \ge 0$, the solutions v_{p1} and v_{p2} are real. However, if $\lambda_1 < 0$, the first two solutions are discarded. After checking the constraint in (28), v_{p1} and the corresponding blend times are calculated and verified. If the first solution satisfies both constraints in (27) and (28),

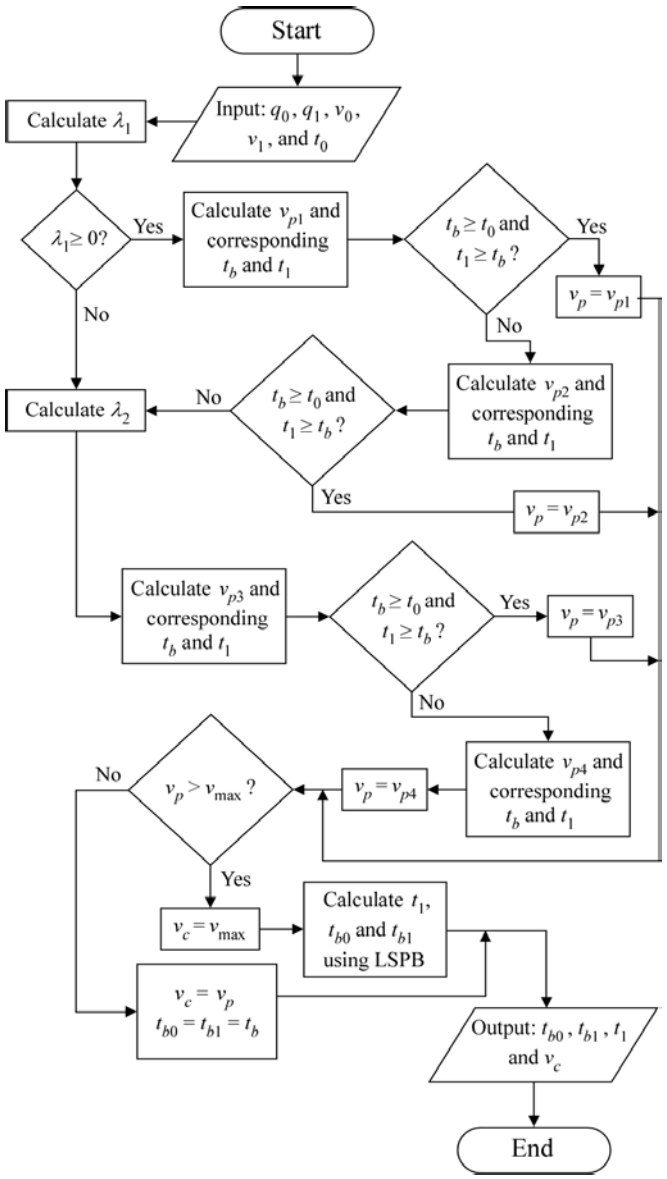

Fig. 5. Flowchart for MTT planning for single degree of freedom motion control.

the results are returned, but if not, v_{p2} is considered. If none of the first two solutions satisfy the constraints, one of the final two solutions, v_{p3} and v_{p4}, will be an acceptable solution. This is because one of the four solutions will always produce a peak velocity. Therefore, the sign of λ_2 does not need to be confirmed. If the value exceeds the maximum possible speed of the motion stage, LSPB trajectory planning is implemented using $v_{\max}$ as the constant velocity v_c. However, if the calculated peak velocity is less than the maximum velocity, the MTT does not include a constant velocity region. However, to unify the output results, v_c will be set equal to v_p, and the blend times t_{b0} and t_{b1} will be equated to t_b.

B. MTT for Two Degrees of Freedom Motion

The solution for the minimum end time presented in the previous section considers only single degree of freedom motion. When determining a MTT for the XY-motion stage, each degree of freedom motion begins at the same initial time

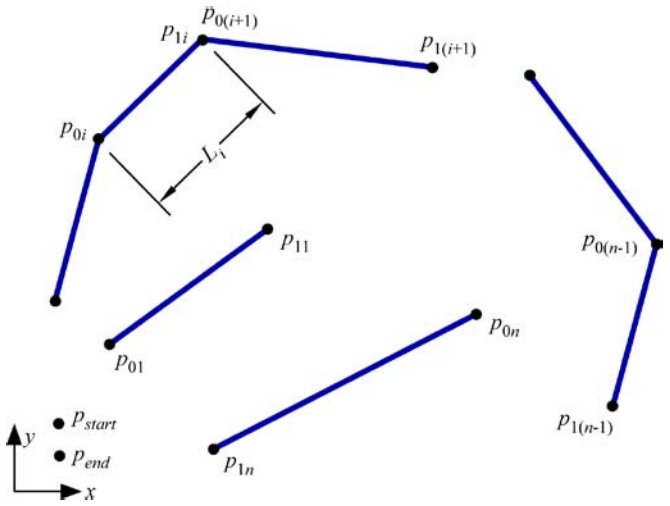

Fig. 6. Parameters used to define desired printing path.

t_0 and ends at the same final time t_1. Therefore, to synchronize time of arrival, the MTT for two degrees of freedom motion is dictated by the slowest degree of freedom, such that

$$t_1 = \max(t_1^X,\ t_1^Y) \tag{39}$$

where t_1^X and t_1^Y are the minimum end times for the X- and Y-motion stages, respectively. The individual end times can be calculated using the MTT algorithm developed for single degree of freedom motion. Once t_1^X and t_1^Y are calculated, the overall minimum end time t_1 can be determined by (39). If $t_1^X \neq t_1$ or $t_1^Y \neq t_1$, the trajectory for the corresponding degree of freedom can be reestablished using the LSPB path planning method according to the now known t_1.

V. Print Path Planning Algorithm

In this section, a new path planning algorithm is developed by combining LSPB and MTT.

A. Preparation for Printing

Before planning a trajectory, printing patterns and paths defined by the user need to be reduced to a set of line segments. Each print line segment can be fully defined by a starting point p_0, an end point p_1, and a desired print speed v_{desired}. Thus, for n line segments, $2n$ points, and n desired speeds describe the entire print region. An example situation is shown in Fig. 6, where the motion stage begins at a starting position p_{start}, moves to p_{01} and deposits material at desired speed v_{desired} until reaching p_{11}. If p_{02} and p_{11} coincide, the shutter remains open and continues printing until reaching p_{12}. Otherwise, the shutter closes, and the motion stage transitions to p_{02} following a MTT. The same procedure will continue until reaching the end point of line n, p_{1n}. Finally, the motion stops at p_{end}.

B. Desired Velocity Components

For path planning, desired velocity of each motion stage should be calculated first. The desired velocity vector, $\mathbf{v}_{i,\text{desired}}$ for the ith line segment can be decomposed into the x- and y-velocity components such that

$$\mathbf{v}_{i,\text{desired}} = v_{xi}\hat{\mathbf{i}} + v_{yi}\hat{\mathbf{j}} \tag{40}$$

where v_{xi} and v_{yi} are the x- and y-velocity components, respectively. Then, the desired speed relates to the velocity components by

$$v_{i,\text{desired}} = \sqrt{v_{xi}^2 + v_{yi}^2}. \tag{41}$$

For 2-D planar motion provided by perpendicular linear motion stages, each desired velocity component directly corresponds to the velocity of each actuator. Due to the relatively low speed and low inertia of the motion stages, the dynamic effects are ignored in this paper.

When two end points p_{0i} and p_{1i} are defined, v_{yi} can be calculated based on the slope of the ith line segment such that

$$v_{yi} = m v_{xi} \tag{42}$$

where

$$m = \frac{y_{1i} - y_{0i}}{x_{1i} - x_{0i}}. \tag{43}$$

By substituting (42) into (41) and assuming $x_{0i} \neq x_{1i}$, the following velocity can be obtained for the x motion:

$$v_{xi} = \pm\frac{v_{i,\text{desired}}}{\sqrt{1+m^2}}. \tag{44}$$

Based on the x-coordinates x_{0i} and x_{1i}, the sign of v_{xi} can be determined by

$$v_{xi} = \text{sgn}(x_{1i} - x_{0i})\frac{v_{i,\text{desired}}}{\sqrt{1+m^2}}. \tag{45}$$

The constant velocity in the y direction v_{yi} can finally be calculated according to (42).

For the case where $x_{0i} = x_{1i}$, the velocity components can be determined by

$$v_{xi} = 0 \tag{46}$$

and

$$v_{\text{yi}} = \text{sgn}(y_{1i} - y_{0i})v_{i,\text{desired}}. \tag{47}$$

C. Path Planning Algorithm

Consider a single segment where the segment's starting point p_{0i} does not coincide with the previous segment's end point $p_{1(i-1)}$, and the target point p_{1i} does not coincide with $p_{0(i+1)}$. The desired printing speed can be maintained over the entire isolated segment only if the average velocity and velocities at p_{0i} and p_{1i} are constrained to $v_{i,\text{desired}}$. Therefore, the boundary velocities become

$$v_{x0i} = v_{x1i} = v_{xi} \tag{48}$$

and

$$v_{y0i} = v_{y1i} = v_{yi} \tag{49}$$

where v_{x0i} and v_{y0i} are the x- and y-velocity components at point p_{0i}, and v_{x1i} and v_{y1i} are the x- and y-velocity

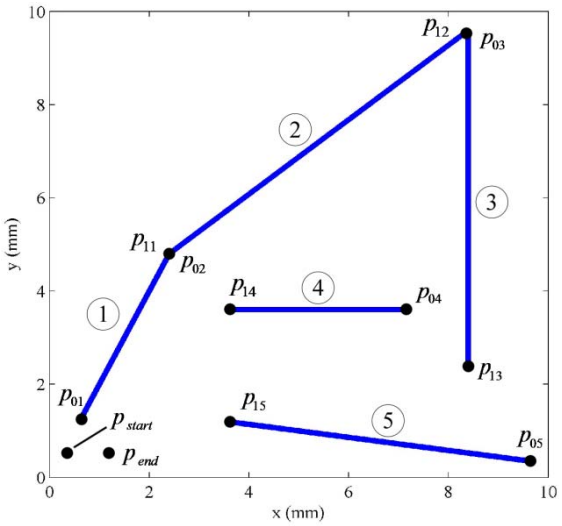

Fig. 7. Set of print segments used for path planning simulation.

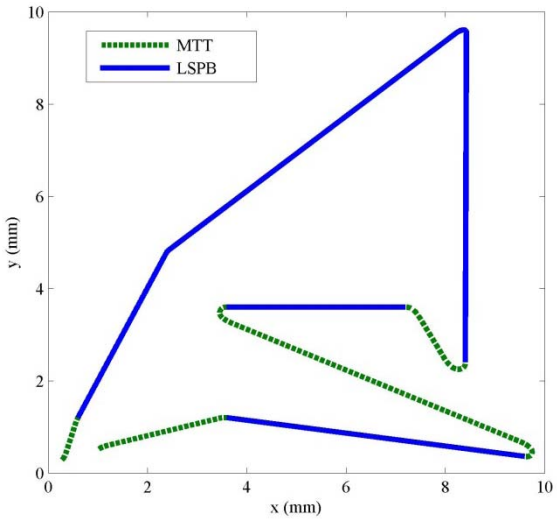

Fig. 8. Planned trajectory of XY-motion stage.

components at point p_{1i}. When printing at the desired velocity, the time required to print the ith segment t_i becomes

$$t_i = \frac{L_i}{v_{i,\text{desired}}} \tag{50}$$

where

$$L_i = \sqrt{(x_{1i} - x_{0i})^2 + (y_{1i} - y_{0i})^2}. \tag{51}$$

After determining the desired x- and y-velocity components and print time for each line segment, a trajectory is planned from p_{start} to p_{end} through each line segment. Velocities at p_{start} and p_{end} are assumed to be zero while the x- and y-motion velocities are determined according to the desired segment velocities v_{x0i}, v_{y0i}, v_{x1i}, and v_{y1i}. If consecutive print segments share a point, the x and y velocities at the joint point are determined as an average such that

$$v_{x1i} = v_{x0(i+1)} = \frac{v_{xi} + v_{x(i+1)}}{2} \tag{52}$$

and

$$v_{y1i} = v_{y0(i+1)} = \frac{v_{yi} + v_{y(i+1)}}{2}. \tag{53}$$

If two consecutive points do not share the same position, the x and y velocities remain constrained to the desired values.

The positions, velocities, and transition times during printing satisfy necessary constraints for LSPB trajectory planning. However, when transitioning between print segments, the motion is planned by the MTT. Since the printing is suspended by the shutter during the transition period, the transition time should be minimal to reduce the overall printing time and material waste.

VI. Simulation of Path Planning Algorithm

To demonstrate the proposed algorithm, a path was planned for the set of print segments shown in Fig. 7. The connected segments ($i = 1, 2$, and 3) are printed continuously, but the two isolated segments ($i = 4$ and 5) require two shutter actuations: opening and closing. By assuming the maximum possible

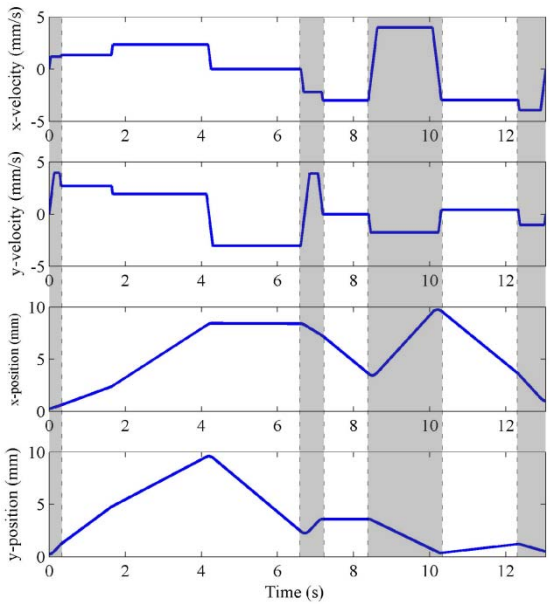

Fig. 9. Velocity and position profiles of x- and y-motion stages. Gray area represents transition periods using MTT.

velocity of 4 mm/s for the XY-motion stage, maximum acceleration of 30 mm/s^2, and desired speed of 3 mm/s for each segment, position and velocity of the motion stage were calculated using the LSPB and MTT methods. As shown in Figs. 7 and 8, the trajectory begins at rest at p_{start}, transitions to the starting point of segment 1 using a MTT, and continuously follows the requirements for the first three segments using LSPB planning. After the shutter closes at point p_{13}, the XY-motion stage executes a MTT to match the velocity and position at p_{04}. Then, the stage maintains a constant velocity while sweeping over segment 4, and the procedure for segment 4 is repeated for the final segment. Finally, the shutter closes at p_{15}, and the motion stage follows a MTT to p_{end} where motion ceases.

The velocities and resulting positions of the motion stages are shown in Fig. 9, where the gray region represents the

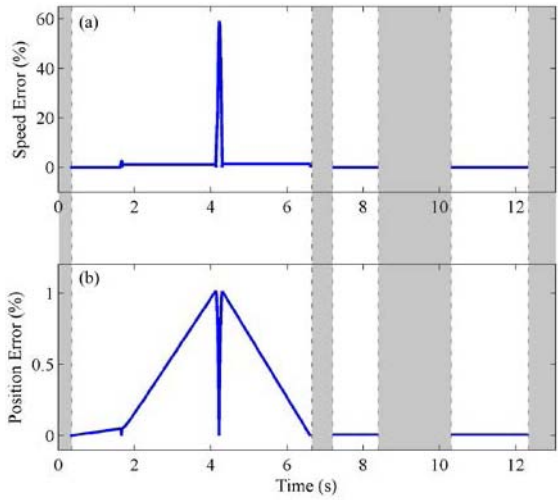

Fig. 10. (a) Speed error and (b) relative position error resulting from planned trajectory. Gray area represents transition periods using MTT.

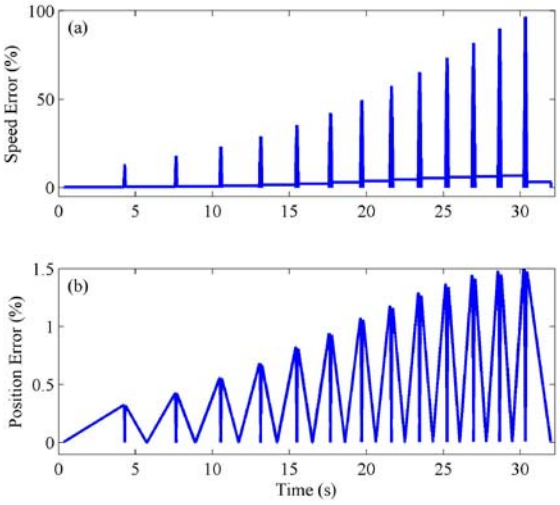

Fig. 12. (a) Speed error and (b) relative position error resulting from decreasing segment angles.

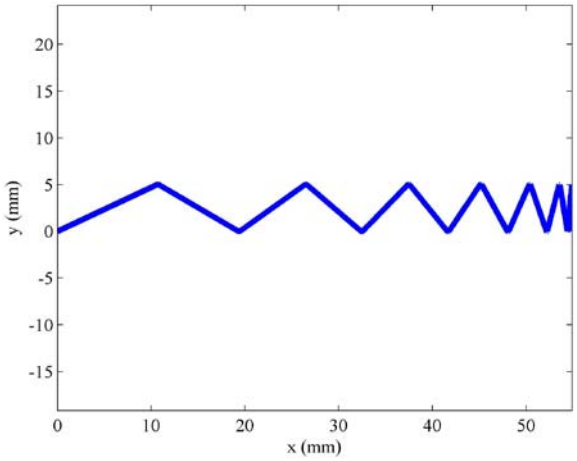

Fig. 11. Trajectory with decreasing segment angles.

transition periods during which the MTT method is applied. Note the trapezoidal shape of the x and y-velocity profiles and the absence of a triangular shape during MTT. Due to the rapid acceleration and relatively long distance between transition points, either the x- or y-motion stage reaches the maximum velocity (4 mm/s) for each MTT. Therefore, the MTT becomes a LSPB trajectory with $v_c = v_{\max}$. Note also that velocity changes during printing (white region) occur only when printing continuous segments 1, 2, and 3, whereas the desired velocities are achieved for segments 4 and 5. For the isolated segments (segments 4 and 5), desired velocities can be matched at each end point by the MTT method. However, at the joint points of the connected segments, velocities are averaged according to (52) and (53), producing speed error.

According to Fig. 10(a), the resulting trajectory produces a large (near 60%) error in speed when transitioning from segment 2 to segment 3. The path is constrained to pass through the point $p_{12} = p_{03}$, and the acute angle created by the two segments requires a large change in the velocities. During the deceleration of the x and y motion, the desired speed (3 mm/s) cannot be maintained. A similar behavior can be observed for segments 1 and 2, but the error is significantly less due to the large angle. The maximum position error, as shown in Fig. 10(b), is less than 1.1 percent of the overall 10-mm feature size.

The angle formed by adjoining segments affects the trajectory velocity and position error. To examine an angle's contribution to errors, a second trajectory shown in Fig. 11 was planned using the velocity and acceleration constraints defined previously. The pattern contains 14 line segments, and beginning at the origin, the segments form angles starting at 125° and decrease linearly to 5°. The peak velocity error shown in Fig. 12(a) increases as angle decreases. With the x- and $y-$velocities averaged at each connection point [(52) and (53)], the abrupt change in motion results in a significant velocity error. For example, a complete change in direction or a 0° angle results in a 100% error. Position error shown in Fig. 12(b) is less of an issue as it does not exceed 1.5%. Because the LSPB method requires the path be constrained to pass through each key point, the trajectory deviates slightly from the straight path, and deviation increases as the angle formed by two segments decrease.

VII. Conclusion

In this paper, a new path planning algorithm was developed for the control of an XY-motion stage in an aerosol printing system. The algorithm is based on two motion control methods: LSPBs and MTT. The path planning algorithm utilizes the two methods to maintain a constant desired speed as much as possible during printing. Specifically, the LSPB method is applied during printing to maintain a desired average speed, and the MTT method is used when transitioning between print segments to minimize transition time. To evaluate the proposed algorithm, x and y trajectories were produced for an arbitrary set of print segments. The results show that the error in relative speed during printing could be large when the stage motion traces connected segments having an acute angle. However, the

actual position deviates little from the desired path. Therefore, to closely maintain the desired motion speed during printing, an improved algorithm will need to be developed in future work.

REFERENCES

[1] I. Gibson, D. W. Rosen, and B. Stucker, *Additive Manufacturing Technologies: Rapid Prototyping to Direct Digital Manufacturing*. New York, NY, USA: Springer-Verlag, 2009.

[2] T. Page, *Design for Additive Manufacturing: Guidelines for Cost Effective Manufacturing*. Berlin, Germany: Lambert Academic Publishing, 2012.

[3] H. Lipson and M. Kurman, *Fabricated: The New World of 3D Printing*. Hoboken, NJ, USA: Wiley, 2013.

[4] E. Cantatore, *Applications of Organic and Printed Electronics: A Technology-Enabled Revolution*. New York, NY, USA: Springer-Verlag, 2013.

[5] V. Subramanian *et al.*, "Progress toward development of all-printed RFID tags: Materials, processes, and devices," *Proc. IEEE*, vol. 93, no. 7, pp. 1330–1338, Jul. 2005.

[6] S.-H. Hur, C. Kocabas, A. Gaur, O. O. Park, M. Shim, and J. A. Rogers, "Printed thin-film transistors and complementary logic gates that use polymer-coated single-walled carbon nanotube networks," *J. Appl. Phys.*, vol. 98, no. 11, p. 114302, 2005.

[7] T. Mustonen *et al.*, "Controlled Ohmic and nonlinear electrical transport in inkjet-printed single-wall carbon nanotube films," *Phys. Rev. B*, vol. 77, no. 12, pp. 125430-1–125430-7, 2008.

[8] R. Liu *et al.*, "All-carbon-based field effect transistors fabricated by aerosol jet printing on flexible substrates," *J. Micromech. Microeng.*, vol. 23, no. 6, p. 065027, Jun. 2013.

[9] H. A. Gieser *et al.*, "Rapid prototyping of electronic modules combining Aerosol printing and ink jet printing," in *Proc. 3rd Electron. Syst.-Integr. Technol. Conf.*, Berlin, Germany, Sep. 2010, pp. 1–6.

[10] S. Park, M. Vosguerichian, and Z. Bao, "A review of fabrication and applications of carbon nanotube film-based flexible electronics," *Nanoscale*, vol. 5, no. 5, pp. 1727–1752, Nov. 2013.

[11] B. Thompson and H.-S. Yoon, "Aerosol-printed strain sensor using PEDOT:PSS," *IEEE Sensors J.*, vol. 13, no. 11, pp. 4256–4263, Nov. 2013.

[12] B. Thompson and H.-S. Yoon, "Aerosol printed carbon nanotube strain sensor," *Proc. SPIE, Smart Sensor Phenomena, Technol., Netw., Syst. Integr.*, vol. 8346, p. 83461C, Mar. 2012.

[13] B. Ando and S. Baglio, "All-inkjet printed strain sensors," *IEEE Sensors J.*, vol. 13, no. 12, pp. 4874–4879, Dec. 2013.

[14] M. Maiwald, C. Werner, V. Zoellmer, and M. Busse, "INKtelligent printed strain gauges," *Sens. Actuators A, Phys.*, vol. 162, no. 2, pp. 198–201, Aug. 2010.

[15] D. Zhao, T. Liu, M. Zhang, R. Liang, and B. Wang, "Fabrication and characterization of aerosol-jet printed strain sensors for multifunctional composite structures," *Smart Mater. Struct.*, vol. 21, no. 11, p. 115008, Nov. 2012.

[16] M. W. Spong, S. Hutchinson, and M. Vidyasagar, "Path and trajectory planning," in *Robot Modeling and Control*. Hoboken, NJ, USA: Wiley, 2005.

Bradley Thompson received the B.S. and M.S. degrees in mechanical engineering from Tennessee Technological University, Cookeville, TN, USA, in 2009 and 2012, respectively. He is currently pursuing the Ph.D. degree in mechanical engineering with the University of Alabama, Tuscaloosa, AL, USA.

His current research interests include modeling, simulation, and control of automotive systems, sensors, and actuators.

Hwan-Sik Yoon received the B.S. degree in physics education from Seoul National University, Seoul, Korea, in 1994, and the M.S. and Ph.D. degrees in mechanical engineering from Ohio State University, Columbus, OH, USA, in 1998 and 2002, respectively.

He joined the Faculty of Mechanical Engineering at the University of Alabama, Tuscaloosa, AL, USA, in 2012, after five years of serving as a Faculty Member with Tennessee Technological University, Cookeville, TN, USA. He is an Assistant Professor with the Department of Mechanical Engineering, University of Alabama. He has authored over 40 research publications in peer-reviewed journals and conference proceedings. His current research interests include smart materials and structures, mechanical sensors and actuators, and modeling, simulation, and control of automotive systems.